Renewable Energy 232 (2024) 120967

Contents lists available at ScienceDirect

Renewable Energy

journal homepage: www.elsevier.com/locate/renene

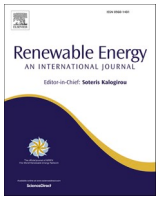

A holistic methodology for designing novel flat plate evacuated solar thermal collectors: Modelling and experimental assessment

Giovanni Barone [a,*], Annamaria Buonomano [a,b], Soteris Kalogirou [c], Panayiotis Ktistis [c], Adolfo Palombo [a]

[a] Department of Industrial Engineering - University of Naples Federico II, P.le Tecchio, 80, 80125, Naples, Italy
[b] Department of Building, Civil and Environmental Engineering - Concordia University, 1455 De Maisonneuve Blvd. W, Montreal, Canada
[c] Department of Mechanical Engineering and Materials Science and Engineering, Cyprus University of Technology, 30 Archbishop Kyprianos Str, 3036, Limassol, Cyprus

ARTICLE INFO

Keywords:
Vacuum solar thermal collector
Solar energy
Modelling
Energy performance analysis

ABSTRACT

This paper presents a comprehensive analysis of the design, implementation, experimentation, and optimization of a novel evacuated flat-plate solar thermal collector characterized by a vacuum level between the glass cover and the absorber plate. The paper addresses different research themes, primarily focusing on developing a low-cost evacuated solar thermal collector with a high innovation level. Additionally, it introduces a comprehensive approach for the conceptualization, design, fabrication, testing, and optimization of solar thermal collectors. Specifically, this study aims to highlight the characteristics of a vacuum-enhanced solar thermal collector and demonstrate a step-by-step process involved in its design, fabrication, testing, and optimization. The proposed methodology is based on the adoption of two software tools and an extensive experimental analysis: the commercial software ANSYS is utilized for structural analysis, while MatLab is employed to develop a suitable mathematical tool for assessing the energy performance of the system and optimizing it. The outcomes show the reliability of the methodology and the performance of the low-cost evacuated solar thermal collector under different vacuum levels, providing insights into energy, economic, and environmental aspects. This work innovates by presenting a thorough analysis covering all solar thermal collector production phases, from conceptualization to optimization. The conclusions highlight the production of a reliable approach, and proof-of-concept results demonstrate how increasing the vacuum level enhances the thermal efficiency of a solar collector.

1. Introduction

The need for innovative renewable energy technologies is increasing on a global scale, as demonstrated by the notable growth in world energy consumption [1] and the alarming rise in greenhouse gas emissions [2], both of which significantly worsen the pressing issue of climate change [3]. This concerning trend is mostly due to the extensive usage of fossil fuels in many different economic sectors, such as industry [4], electricity and heat production [5] transportation systems [6,7], urban communities [8,9], island communities [10,11], infrastructure [12,13], etc.

Scientists and researchers strongly support sustainable energy transitions, emphasizing the need to prioritize energy-efficient solutions [14], and to strategically adopt renewable energy sources [15,16]. Nowadays, other than fossil fuel, many alternative solutions allow for producing energy from natural sources, such as solar energy [17], wind [18], geothermal [19,20], hydropower [21], ocean energy [22], and bioenergy [23]. However, solar energy is the most abundant and easily to be exploited [24]. Therefore, its exploitation is essential to the paradigm shift towards sustainable energy systems [25]. Due to its inherent flexibility, solar energy can be converted into power or heat using various methods [26].

Over the past three decades, there has been a significant increase in scientific publications focused on the utilization of solar energy [27]. This research has led to the identification and classification of different types of solar collectors based on a range of features, including their geometry [28], elements used [29], the type of output they provide, such as electricity, heat, or both [30], the heat transfer fluid they adopt [31], and many other features [32]. Solar thermal collectors are designed to convert solar energy into heat, which can then be used to provide hot air [33], hot water [34], or just for directly supplying heat to a fluid (e.g. in direct solar-assisted heat pumps [35]). Furthermore, these

* Corresponding author.
E-mail address: giovanni.barone@unina.it (G. Barone).

https://doi.org/10.1016/j.renene.2024.120967
Received 29 December 2023; Received in revised form 20 May 2024; Accepted 9 June 2024
Available online 28 July 2024

systems can be adopted in stand-alone configuration or can be adopted as part of the building envelope [36,37]. While many studies have proposed enhancements to these systems, it is clear from the scientific literature that most of these have focused only on specific cases and features. To develop high performance solar thermal collectors, a holistic approach is needed that simultaneously considers many aspects of the design and implementation of a solar thermal collector prototype. In this paper, a novel step-by-step procedure that considers all possible factors during all stages of the design, implementation, experimentation, and optimization of a novel solar thermal collector.

1.1. Literature review

When solar energy is adopted for meeting the heating needs for air conditioning or domestic hot water preparation, evacuated tube collectors are one of the most often used types, accounting for around 70 % of solar-powered systems installed worldwide [38,39]. This prevalence can be attributed to high thermal efficiency with a low gross area occupation [40]. However, flat-plate solar thermal collectors are characterized by a simpler geometry and more straightforward installation and maintenance procedures compared to evacuated tube collectors [32]. Specifically, these systems represent a highly adaptable and efficient choice, encompassing advantages that span from easy integration into diverse applications to the inherent simplicity of their design [32]. Basically, flat-plate solar thermal collectors comprise an absorbent surface suitably engineered to capture solar radiation. Subsequent to the absorption of solar energy, it undergoes conversion into heat, which is efficiently transmitted to a heat transfer fluid circulating externally to the absorbent surface [41]. The primary limitation of a flat-plate collector stems from convective heat losses occurring between the absorber plate and the glass cover, in the case of a glazed collector, or the outdoor environment, in the case of an unglazed collector [42]. This is another reason why evacuated tube collectors are preferred instead of flat plate solar thermal collectors [43]. A promising solution to fill this gap is developing a flat plate solar thermal collector with vacuum technology [44]. This approach allows remarkably containing the convective motions occurring in the collector and the relative heat losses with a consequential increase in the thermal energy efficiency of these systems [45]. However, a vacuum cavity is critical to be realized for flat shapes, whereas the technical realization is easier for cylindric geometry [46], but in the case of cylindrical geometry, a loss of gross receiving area is obtainable with a consequential reduction in terms of the total amount of energy converted [47]. Therefore, the study of this kind of system also under the mechanical and stress point of view is crucial for obtaining a high performed flat-plate solar thermal collector [48].

A comprehensive body of scientific literature exists about various aspects of flat plate solar thermal collectors [33]. In particular, diverse methodologies and strategies associated with all constituent elements involving flat plate solar thermal collectors have been thoroughly examined and documented [49]. Moreover, numerous methodologies have been used to evaluate the effectiveness of these enhanced solutions, ranging from simulation-based analyses to experimental investigations [50–53]. A significant point to consider is whether vacuum insulation between the absorber plate and the glass cover can be accomplished. This approach serves to mitigate convective heat losses within the system. Various alternatives exist for realizing this goal. The easier way to seal the glass cover on the absorber plate is the adoption of a silicon film [54]. However, this solution allows for obtaining quite low vacuum levels because it requires more strength than an adhesive bond vacuum-seal [55]. Therefore, for this application other solutions such as innovative materials adopted for sealing electronic materials are adoptable. A sealing system, employing a tin-based alloy known as Cerasolzer 217, exhibits commendable optical and thermal characteristics, rendering it a viable sealing method [56]. In particular, this solution imparts durability to the system by its elevated mechanical strength and effective resistance to airtightness leaks [57]. Another solution is represented by laser glass frit sealing, which is a prominent joining method widely adopted in electronics [58]. This solution is adapted to laser glass frit sealing, traditionally used for display panels, to encapsulate vacuum insulation glass. However, to realize this sealing and avoid cracks, precise thermal management is required [59]. Whether the formation of a vacuum is attributable to one solution rather than another, prototyping a system utilizing vacuum technology for thermal insulation requires a comprehensive examination of both material and geometry [60]. This phenomenon is specifically induced by the mechanical stresses to which the components are subjected, and any mistake in properly sizing may result in the implosion of the panel. Therefore, a mechanical stress analysis is required to properly design all elements composing the solar thermal collectors [61]. Various approaches were explored to harness the benefits of vacuum insulation while maintaining the straightforward design of flat-plate solar collectors. One possible solution is the adoption of a curved cover, enabling the achievement of robust vacuum insulation. This approach could result in substantial thermal efficiency gains of 7.13 % and 28.32 % when compared to standard flat plate solar collectors and evacuated tube solar collectors, respectively [62]. This innovative approach shows considerable promise as a cost-effective solution for hot water production, thereby enhancing its viability in diverse settings. Another approach for sustaining the vacuum is the adoption of suitable pillars that prevent the collapse of the glass cover on the absorber plate. However, this approach requires a customized study regarding the proper size of support pillars to minimize thermal bridges and prevent the increase in thermal efficiency, because vacuum insulation is compensated by thermal bridges provided by pillars [60]. Due to the elevated level of vacuum achievable through the proper utilization of pillars and advanced sealing methods, the evacuated solar collectors exhibits a promise potential to generate heat for space heating, during the heating season, and generate steam in the non-heating season. This effectively addresses the issue of seasonal misalignment in traditional solar thermal heating systems [63]. Another widely investigated technology adopted to increase the energy efficiency of solar thermal collectors is the utilization of solar coatings [64]. This solution allows an increase in the absorbance of the solar collector within the solar wavelength spectrum and a simultaneous reduction in emissivity in the infrared wavelength spectrum [65]. A critical aspect in adopting this technology is the deposition of the solar coating layer on the absorber plate. Here, the thickness of the solar coating layer constitutes a crucial factor in increasing energy efficiency of solar thermal collectors [66]. Hence, the installation technique necessary for accurately displacing the layers of solar coating must be meticulously devised to achieve the desired thickness and positioning [67]. Different materials are also adopted in solar coatings [68], however, the most widely and effective used paint is a silicone polymer with xylene solvent [69].

1.2. Motivation

The scientific literature reported in the previous section underlines the need for a detailed research methodology for the design of solar thermal collectors with the integration of innovative technologies. It is evident that the focus within scientific articles is mainly directed towards aspects relating to the conceptualization of innovative solar thermal collectors. Particularly, these articles primarily concentrate on single factors involving technologies, design methodologies, and the optimization of specific parameters. Nevertheless, there is a marked lack of a holistic viewpoint that encompasses the whole range of activities, from the first stages of conceptualization to the latter phases of design, experimentation, and optimization. This significant gap highlights the need of further investigation and integration synthesis of findings throughout all stages of developmental, in order to guarantee a holistic comprehension of the complex dynamics involved in the development of solar thermal collector systems.

To address this gap, a comprehensive research methodology aimed at

conceptualizing, designing, and optimizing novel solar thermal collectors is presented. Furthermore, it is applied to realize a novel low-cost flat plate evacuated thermal collector. The main milestone obtained in this paper are as follows.

- Development of a comprehensive and highly organised methodology that allows for the production and optimization of solar thermal collectors characterized by a high innovation level with low initial costs.
- Implementation of a cost-effective vacuum cavity between the absorber plate and the glass cover that significantly mitigates convective losses to the environment.
- Incorporation of a corrugated shape in the absorber plate that enhances the heat exchange with the pipe risers and facilitates the installation of steel pillars, thereby preventing system implosion.
- To ensure proper system design and the structural integrity of the pillars required to withstand the vacuum, a suitable structural and thermal stress analysis is conducted by using a 3-D geometrical CAD model imported into the ANSYS environment.
- To investigate the energy, economic, and environmental performance of the considered system under diverse operating conditions, a dynamic simulation model based on a resistive-capacitive thermal network is also developed in the MatLab environment.
- Experimental validation of the model is carried out using experimental data collected during an extensive experimental campaign, revealing exceptional agreement between experimental and simulation results.
- The effects of vacuum quality levels on the energy performance of an innovative flat plate solar thermal collector prototype are assessed through a suitable experimental campaign and various simulation results.

To summarize, the novel solar thermal collector produced according to the proposed methodology has great potential in terms of energy efficiency, economic feasibility, and environmental impact.

2. Material and method

In this section, the step-by step procedure adopted for conceptualize, design, test and assess the energy performance of the novel low-cost flat plate evacuated thermal collector prototype is presented. The methodology adopted in this study is reported in Fig. 1. The prototype design procedure starts with the conceptualization of the novel low-cost flat plate evacuated thermal collector prototype, that it is theorized starting from the lacks reported in the literature review, related to previous studies on solar thermal collectors. As reported, the primary goal of this study is to provide a reliable methodology for design solar thermal collectors. The system is coincided for working with high efficiency compared to standard flat plate solar thermal collectors and be cost-effective to manufacture. Therefore, to accomplish this goal, the vacuum technology is selected and to implement it into the system, a suitable preliminary structural analysis is conducted. This analysis is required for define the proper number, size, and dimension of all elements comprising the solar thermal collector prototype. The structural design of the prototype is based on a detailed analysis of the materials and components. The prototype is designed to have an evacuated flat plate design, with a vacuum insulation layer between the absorber plate and the glass cover. The absorber plate is designed to maximize solar radiation absorption and minimize heat losses through conduction and radiation. Further details related to the structural analysis are reported in a separate section. Finally, after sizing all elements composing the solar thermal collector, the prototype is realized by using a combination of sheet metal forming, and artisanal welding techniques.

After that, to properly assess the energy performance of the developed prototype and develop a suitable instrument tool able to optimize the energy performance of the prototype, a suitable dynamic simulation model is written in MatLab environment. The model is based on a three-dimensional resistive-capacitive thermal network and it includes detailed descriptions of the radiation and conduction heat transfer mechanisms. Thus, to assess the reliability of the developed tool and experimentally validate it, an extensive experimental analysis is conducted. The experimental setup used to evaluate the performance of the prototype consists of a set of different thermocouples, flowmeters, pyranometer, data acquisition systems and other test facilities. The performance of the prototype are evaluated under various operating conditions, including different solar radiation and ambient temperatures. Temperature sensors have been installed at various locations on the collector to measure the temperature distribution and to experimentally assess the heat transfer rate. The experimental data obtained from the thermal test facility are compared with the predictions of the simulation model. The agreement between the experimental data and the simulation results has been found to be excellent, indicating that the model accurately simulate the performance of the collector under different operating conditions. In the following, details regarding all the steps adopted in the proposed methodology are provided in suitable subsections.

2.1. Conceptualization

In this section, the development of the novel low-cost flat plate evacuated thermal collector prototype is presented. The collector is composed of six distinct elements, as illustrated in Fig. 2a. These include

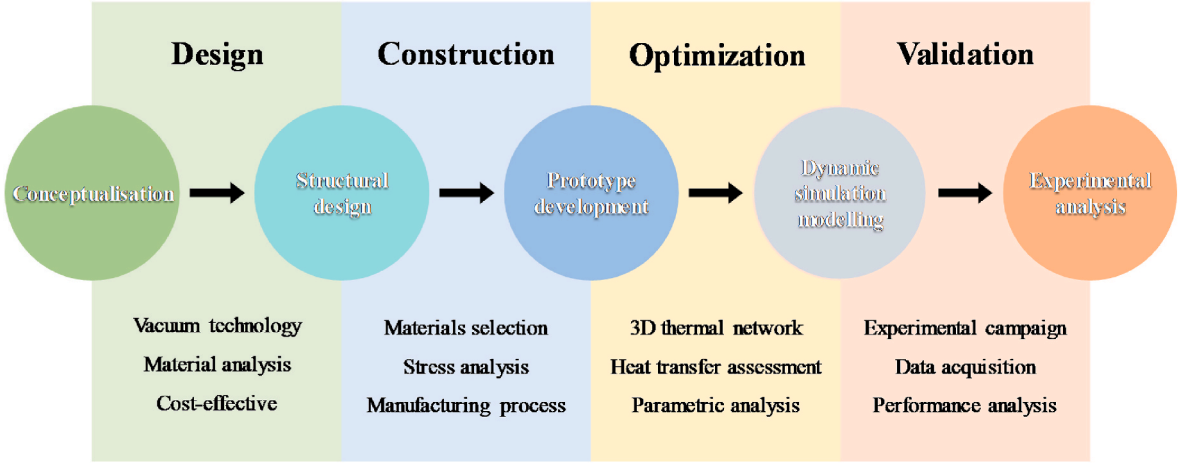

Fig. 1. Methodology adopted for conceptualize, design, test the novel evacuated flat plate solar thermal collector prototype.

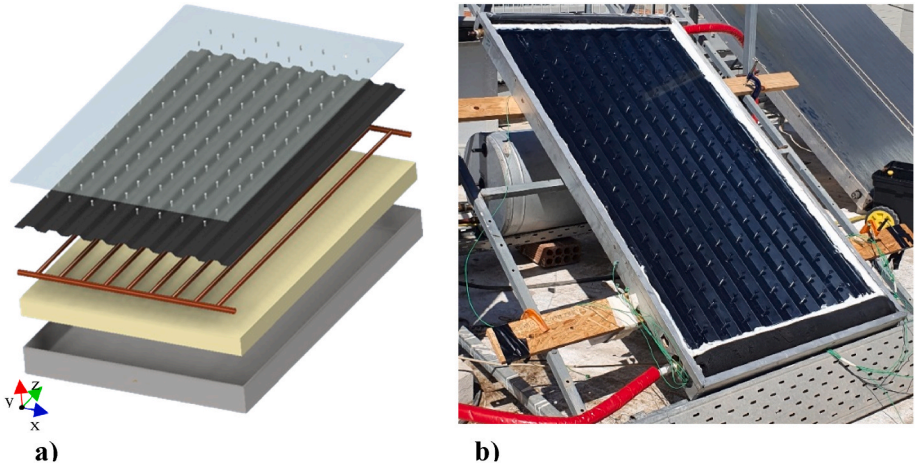

Fig. 2. Sketches of the developed solar thermal collector: a) 3D geometrical model; b) physical prototype.

a glass cover with dimensions of 1.50 m length (l_{glass}), 0.97 m width (w_{glass}), and 8.0 mm thickness (t_{glass}), with a gross area of 1.46 m^2 (A_{glass}). The collector also contains a set of eight rows of eighteen hexagonal screws with a diameter of 19.1 mm (D_{pillar}) and a length of 0.40 m (l_{pillar}); a corrugated metal sheet used as an absorber plate with dimensions of 1.51 m length (l_{plate}), 0.96 m width (w_{plate}), and 4.0 mm thickness (t_{plate}); a set of two headers with a diameter of 19.0 mm (D_{header}) and a length of 1.00 m (l_{header}); nine risers with a diameter of 12.7 mm (D_{riser}). Moreover, an insulated plate with dimensions of 1.80 m length (l_{ins}), 0.80 m width (w_{ins}), and 80 mm thickness (t_{ins}) and an edge cover with dimensions of 2.10 m length (l_{edg}), 1.15 m width (w_{edg}), and 6.0 mm thickness (t_{edg}) are included in the prototype assembly to shape the collector, as shown in Fig. 2b.

To form the pipes system for heat exchange, the two headers are welded to the nine risers, and the pipes system is then welded to the bottom face of the absorber plate. Furthermore, the glass cover is sealed to the absorber through a suitable silicon bonding row.

2.2. Structural design

The structural analysis of the novel low-cost flat plate evacuated thermal collector prototype is conducted by initially prototyping the system using Creo Parametric 3D Modelling Software [70] and ANSYS Workbench Platform software [71]. Initially, a suitable three-dimensional geometrical model is developed and imported into ANSYS for static structural analysis under varying levels of vacuum inside the collector. The objective of this preliminary analysis is to assess the reliability of the number of pillars, as well as define the optimum thickness of both glass cover and absorber plat needed to withstand the desired vacuum level. The sketch of the three dimensional geometrical model with the relative mesh grid for the novel evacuated flat plate solar thermal collector is reported in Fig. 3.

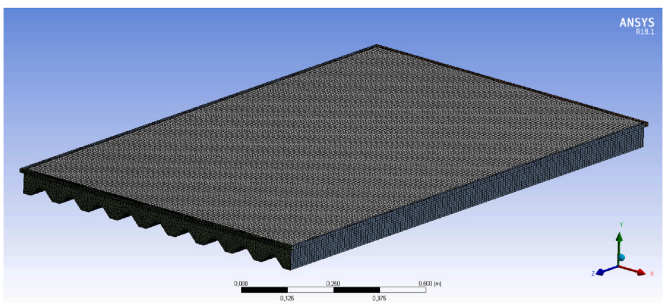

Fig. 3. Mesh for structural analysis: adaptive size with a characteristic size of $1.764 \bullet 10^{-4}$ mm.

Here, an adaptive geometry with a maximum characteristic size of 1.764×10^{-4} mm is utilized, as it is determined to be a suitable trade-off between the computational time and the results reliability. Based on the dimensions provided in the *Conceptualization* section, the structural analysis is conducted with an 8.0 mm thickness of glass cover, a 4.0 mm thickness of absorber plate, and a total of 144 pillars arranged in 8 rows with 18 strips each. In Fig. 4 displays the results of the structural analysis for both the absorber plate and the glass cover.

The left side of Fig. 4 illustrates the mechanical deformations observed in the absorber plate, while the right side presents the deformations observed in the glass cover. The structural analysis is conducted at three different vacuum quality levels with eight different pressure levels: low-vacuum pressure (i.e. between 10^{-1} and 10^{-2} mbar, top figures), medium-vacuum pressure (i.e., between 10^{-3} and 10^{-6} mbar, middle figures), and high-vacuum pressure (i.e., between 10^{-7} and 10^{-8} mbar, bottom figures). The figures demonstrate that higher vacuum pressure levels result in greater mechanical deformations. The maximum mechanical stress (σ_{max}) and corresponding deformation (ε_{max}) occur at the edge of the absorber and the centre of the glass cover. Specifically, a mechanical stress ranging from $6.7 \bullet 10^{-6}$ to $7.2 \bullet 10^{3}$ MPa, with a mechanical deformation ranging from $8.3 \bullet 10^{-6}$ to $1.0 \bullet 10^{2}$ mm, is observed as vacuum pressure increases from low to high. Additional details regarding mechanical stress and deformation can be found in Table 1. This table provides insight into the vacuum quality level achievable with the selected thickness, and for the selected design structure, a medium vacuum (10^{-3} mbar) can be sustained with a deformation of $1.1 \bullet 10^{-3}$ mm.

2.3. Dynamic simulation model

The third step in the methodology involves the development of a suitable dynamic simulation model purposely designed to evaluate the energy, economic, and environmental performance of the novel evacuated flat plate solar thermal collector prototype. The dynamic simulation model is tailored to the conceptualized system, and it is written in MatLab environment. It is intended to be integrated into in-house building energy performance simulation tools to enable diverse analyses concerning the integration of the system into the building envelope and optimize the energy performance by varying different design parameters [72]. The development of the dynamic simulation model starts with the discretization procedure. Here, each element is divided into several sub-volumes and their thermal behavior is evaluated by considering a temperature node for each sub-volume. The discretization procedure involves the absorber plate, the risers, and the volume in which the water flow is included, whereas the glass cover and edge cover

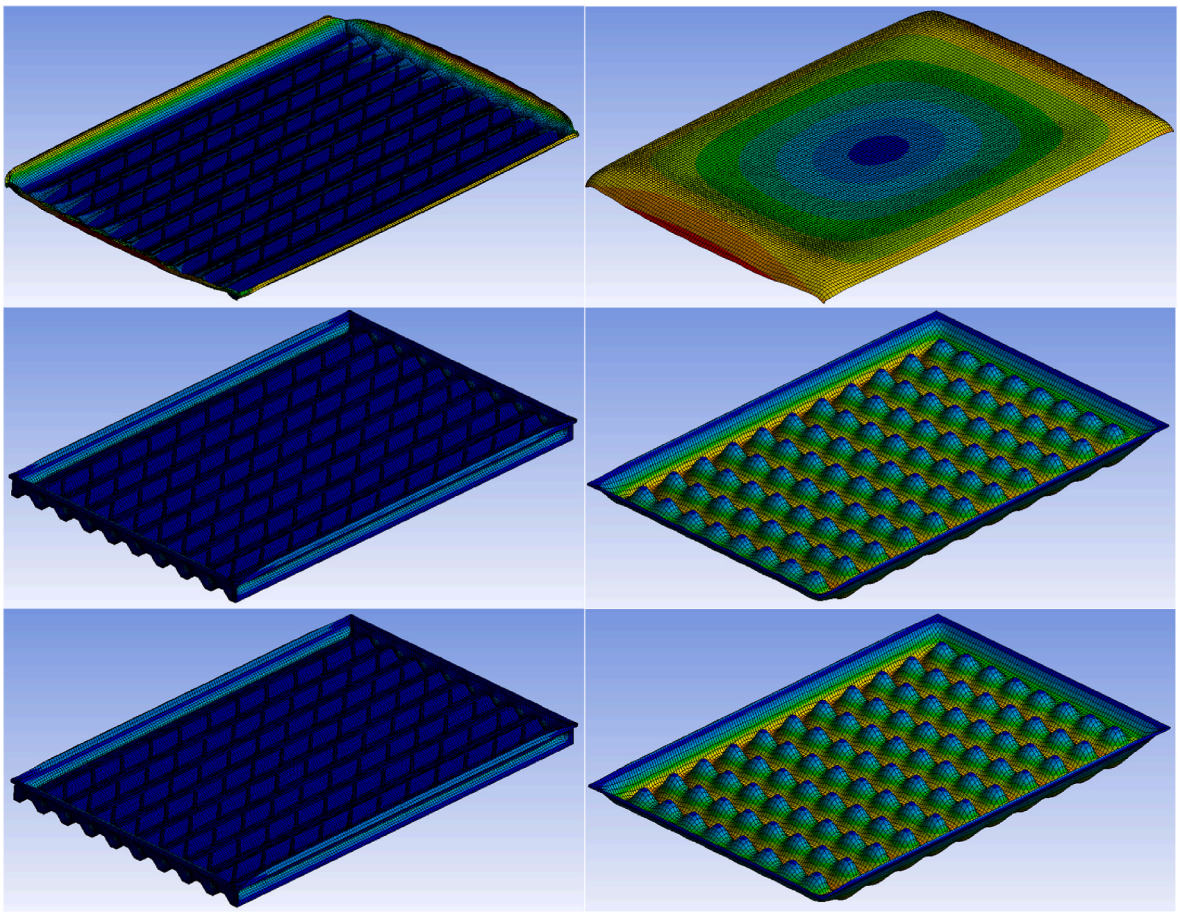

Fig. 4. Total deformation for the absorber plate (left figures) and glass cover (right figures), for low (up), medium (middle), and high vacuum (bottom).

Table 1
Mechanical stress and deformation for each vacuum level.

Vacuum quality	Pressure [mbar]	σ_{max} [MPa]	ε_{max} [mm]
Low	10^{-1}	$6.7\bullet10^{-6}$	$8.3\bullet10^{-6}$
	10^{-2}	$2.3\bullet10^{-5}$	$2.1\bullet10^{-5}$
Medium	10^{-3}	$8.2\bullet10^{-4}$	$5.7\bullet10^{-4}$
	10^{-4}	$5.4\bullet10^{-3}$	$4.3\bullet10^{-3}$
	10^{-5}	$4.2\bullet10^{-2}$	$1.8\bullet10^{-2}$
	10^{-6}	$6.8\bullet10^{-1}$	$1.1\bullet10^{-1}$
High	10^{-7}	$0.8\bullet10^{0}$	$0.3\bullet10^{0}$
	10^{-8}	$1.5\bullet10^{2}$	$1.7\bullet10^{1}$

*Boundary conditions $T_{amb} = 20$ °C, $G_{tot} = 800$ W/m^2 $T_{max,\ absorber} \approx 240$ °C.

are not discretized, and a single temperature is considered for these two elements. Specifically, the discretization procedure is show through the two cross sections (x-y), and (x-z) of the system reported in Fig. 5.

Here, all the elements comprising the prototype can be distinguished and the discretization procedure is clearly defined. Due to the shape of the absorber plate, a discretization technique is employed, where two different configurations are considered. The first configuration involves 10 sub-volumes characterized by the temperature node $T_{abs,d}$, which correspond to the part of the absorber plate in contact with the pillars and insulation. The second configuration involves 9 sub-volumes characterized by the temperature node $T_{abs,u}$, which allow for heat supply to the risers that the water flows through.

This approach is necessary since the absorber plate exchanges heat with two distinct elements (i.e., the risers and the insulation). The primary objective of this system is to maximize the heat exchange between the absorber plate and the risers while minimizing heat losses through

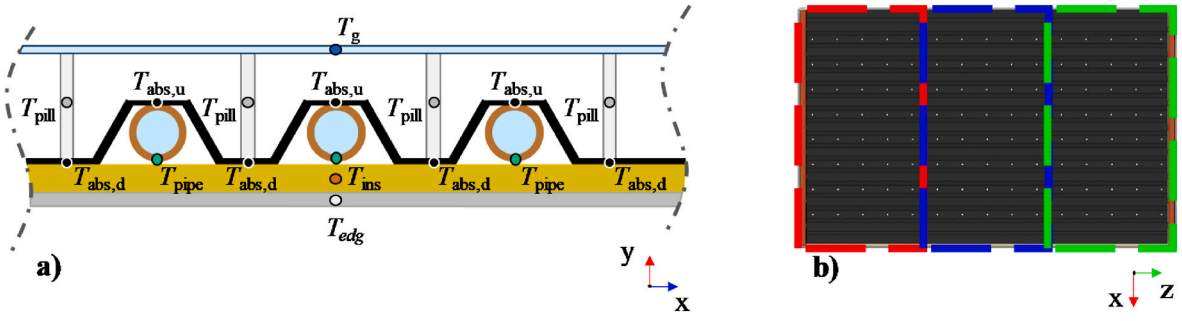

Fig. 5. Cross sections of the solar thermal collector with the relative temperature nodes and sub-volumes.

the insulation, pillars, and vacuum gap cavity. The vacuum gap cavity plays a crucial role in reducing convective heat losses across the system. Furthermore, the temperature nodes along the z-axis, as depicted in Fig. 5b, are categorized into three sub-volumes, namely, the "bottom," "middle," and "upper' sub-volumes, highlighted in red, blue, and green dotted areas, respectively. For the bottom sub-volume, $T_{abs,d,bottom}$ and $T_{abs,u,bottom}$ are defined. Similarly, for the middle and upper sub-volumes, $T_{abs,d,middle}$ and $T_{abs,u,middle}$, as well as $T_{abs,d,upper}$ and $T_{abs,u,upper}$, are defined, respectively. This approach necessitates the use of 19 × 3 temperature nodes to assess the temperature field of the absorber plate. A similar approach is taken for the other temperature nodes along the (x-z) section.

Regarding the risers, each pipe is subdivided into three distinct sub-volumes, namely, $T_{pipe,\ bottom}$, $T_{pipe,\ middle}$, and $T_{pipe,\ upper}$, requiring a total of 9 × 3 temperature nodes to evaluate the temperature distribution along the risers. The pillars are also discretized into eight pillars each for the bottom, middle, and upper sub-volume areas, characterized by $T_{pillar,\ bottom}$, $T_{pillar,\ middle}$, and $T_{pillar,\ upper}$, respectively. Finally, the water flowing into the risers is similarly discretized. However, for the glass cover, insulation, and edge cover, a different discretization approach is employed, where a single temperature node is used for each of the three elements. Consequently, a total of 111 temperature nodes are utilized to assess the temperature.

To evaluate the energy performance of the innovative system, a suitable dynamic simulation model based on a 3D resistive-capacitive thermal network is developed and the relative thermal network is presented in Fig. 6. This methodology facilitates the evaluation of conductive, convective, and radiative heat transfer among the various components of the solar thermal collector.

In Fig. 6, seven distinct temperature node colors can be observed. The light grey temperature node corresponds to the edge cover, while the orange temperature node signifies the insulation layer. The light green temperature node represents the pipe sub-volume, and the black temperature node denotes the absorber pipe. The light blue color is assigned to the glass cover. Furthermore, the weather boundary conditions are represented by dark blue and red nodes, indicating the sky temperature and outdoor air temperature, respectively. Note that, for the sake of clarity, temperature nodes regarding the water flow are not reported in the figure but are included in the energy balance of the system. Furthermore, temperature node referred to the gap cavity is also not reported in the figure, but it is included in the heat exchange phenomena. To assess the temperature distribution across the solar thermal collector, an energy balance analysis is performed for each temperature node using the MatLab dynamic simulation tool.

The temperature of the glass cover is assessed by considering the following equation:

$$C_{glass}\frac{dT_{glass}}{d\theta} = \alpha_{glass}G_{tot}A_{glass} + Q_{c,glass-amb} + Q_{r,glass-sky} + Q_{c,glass-gap} + Q_{k,glass-pillars} + \sum_{n=1}^{k} Q_{r,glass-abs,n} \quad (1)$$

In this equation several parameters are include and described in detail as follow. The thermal capacity of the glass cover, denoted as C_{glass}, the temperature of the glass cover, denoted as T_{glass}, and the timestep of the simulation, denoted as θ. Additionally, the model incorporates the absorbance of the glass cover, denoted as α_{glass}, the incident solar radiation on the glass cover, denoted as G_{tot}, and the surface area of the solar collector, denoted as A_{glass}. Moreover, the model considers several other factors, such as the convective thermal power exchanged between the glass cover and the ambient, denoted as $Q_{c,glass-amb}$, the radiative thermal power exchanged between the glass cover and the sky, denoted as $Q_{r,glass-gap}$, and the convective thermal power exchanged between the glass cover and the gap cavity, denoted as $Q_{c,glass-gap}$. The number of sub-volumes in which the absorber plate is discretized, denoted as k, and the conductive thermal power exchanged between the glass cover and the pillars, denoted as $Q_{k,glass-pillars}$, are also incorporated into the model. Finally, the radiative thermal power exchanged between the glass cover and the nth absorber plate sub-volume is denoted as $Q_{r,glass-abs,n}$.

The temperature of the absorber plate is assessed by considering the following equation:

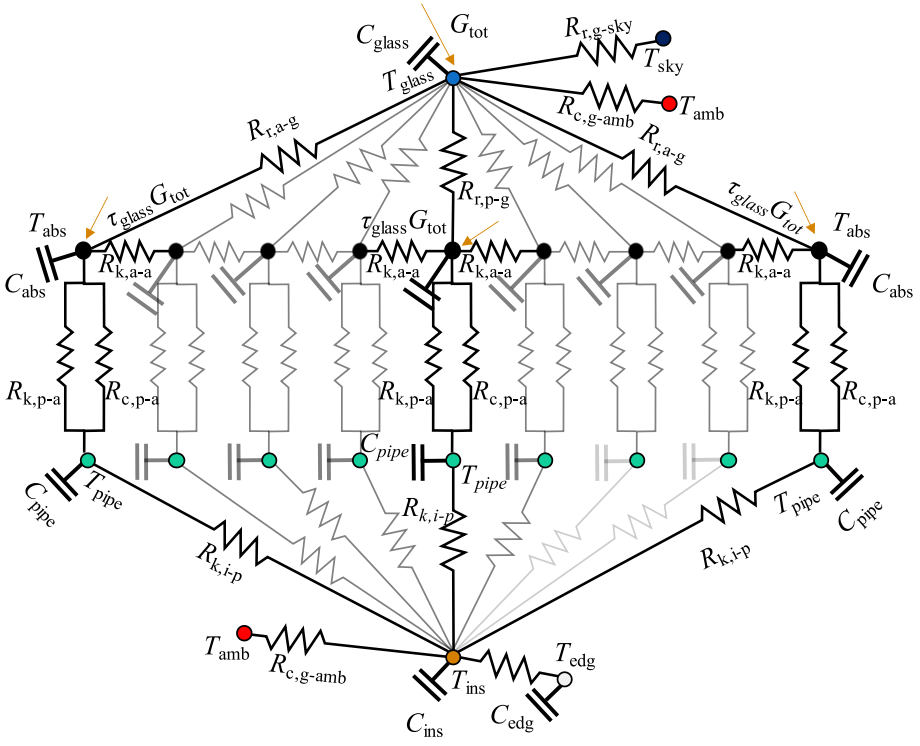

Fig. 6. Resistive-capacitive 3D thermal network.

$$C_{abs,n}\frac{dT_{abs,n}}{d\theta} = \tau_{glass} G_{tot} A_{abs,n} + Q_{k,abs,n-pipe} + Q_{c,abs,n-gap} + Q_{r,abs,n-glass} + \sum_{j=1}^{n-1} Q_{k,abs,n-abs,j} \quad (2)$$

where $C_{abs,n}$, is the thermal capacity of the *n*th sub-volume absorber plate, $T_{abs,n}$ is the temperature of the *n*th sub-volume absorber plate, τ is the transmittance of the glass cover, $A_{abs,n}$ is the surface area of the *n*th sub-volume of the absorber plate, $Q_{k,abs,n\text{-}pipe}$ is the conductive thermal power exchanged between the *n*th sub-volume of the absorber plate and the corresponding pipe placed beyond, $Q_{c,abs,n\text{-}gap}$ is the convective thermal power exchanged between the *n*th sub-volume of the absorber plate and the gap cavity, $Q_{r,abs,n\text{-}glass}$ is the radiative thermal power exchanged between the *n*th sub-volume of the absorber plate and the glass cover, and $Q_{k,abs,n\text{-}abs,j}$ is the conductive thermal power exchanged between the *n*th sub-volume of the absorber plate and the adjacents *j*.

The temperature of the riser pipes is assessed by considering the following equation:

$$C_{pipe,n}\frac{dT_{pipe,n}}{d\theta} = Q_{c,pipe,n-w} + Q_{k,pipe,n-abs} + Q_{k,pipe,n-ins} + \sum_{j}^{\pm 1} Q_{k,pipe,n-pipe,n-j} \quad (3)$$

where $C_{pipe,n}$ is the thermal capacity of the *n*th sub-volume riser pipe, $T_{pipe,n}$ is the corresponding temperature of the sub-volume, $Q_{c,pipe,n\text{-}w}$ is the convective thermal power exchange between the *n*th sub-volume of the riser pipe and the flowing water beyond, $Q_{k,pipe,n\text{-}abs}$ is the conductive thermal power exchange between the *n*th sub-volume of the riser pipe and the absorber plate, $Q_{k,pipe,n\text{-}ins}$ is the conductive thermal power exchange between the *n*th sub-volume of the riser pipe and the insulation layer, and $Q_{k,pipe,n\text{-}pipe,n\text{-}j}$ is the conductive thermal power exchange between the *n*th sub-volume of the riser pipe and the adjacent sub-volume.

The temperature of the insulation layer is assessed by considering the following equation:

$$C_{ins}\frac{dT_{ins}}{d\theta} = \sum_{u=1}^{m} Q_{k,ins-pipe,u} + \sum_{v=1}^{n} Q_{k,ins-abs,v} + Q_{k,ins-edge} \quad (4)$$

where C_{ins} represents the thermal capacity of the insulation layer, T_{ins}, is the temperature of the insulation layer, $Q_{k,ins\text{-}pipe,u}$ is the conductive thermal power exchanged between the insulation layer and *u*th riser pipe, $Q_{k,ins\text{-}abs,v}$ represents the conductive thermal power exchanged between the insulation layer and *v*th sub-volume absorber plate; $Q_{k,ins\text{-}edge}$ is the conductive thermal power exchanged between the insulation layer and the edge cover.

The temperature of the edge cover is assessed by considering the following equation:

$$C_{edge}\frac{dT_{edge}}{d\theta} = Q_{k,edge-ins} + Q_{c,edge-amb} \quad (5)$$

where C_{edge} represents the thermal capacity of the edge cover, T_{edge} is the temperature of the edge cover, $Q_{k,edge\text{-}ins}$ represents the conductive thermal power exchanged between the edge cover and the insulation layer, and $Q_{c,edge\text{-}amb}$ is the convective thermal power exchanged between the edge cover and outdoor air.

The temperature of the fluid included into the gap cavity between the glass cover and the absorber plate is assessed by considering the following equation:

$$C_{gap}\frac{dT_{gap}}{d\theta} = \sum_{v=1}^{n} Q_{c,gap-abs,v} + Q_{c,gap-glass} + Q_{c,gap-pillar} \quad (6)$$

where C_{gap} represents the thermal capacity of the gap cavity, T_{gap} is the temperature of the gap cavity, $Q_{c,gap\text{-}abs,v}$ represents the convective thermal power exchanged between the gap cavity and the *v*th sub-volume absorber plate, $Q_{c,gap\text{-}glass}$ represents the convective thermal power exchanged between the gap cavity and the glass cover, and $Q_{c,gap\text{-}pillar}$ is the conductive thermal power exchanged between the gap cavity and the pillars.

The temperature of the water flowing into the pipe risers is assessed according to the following equation:

$$C_{water}\frac{dT_{water}}{d\theta} = \sum_{j}^{\pm 1} Q_{c,water,j} + Q_{c,pipe-water} \quad (7a)$$

where C_{water} represents the thermal capacity of the water included in the pipe riser, T_{water} is the temperature of the water included in the pipe riser, $Q_{c,water,j}$ is the convective thermal power exchanged between the water included in the pipe riser and the adjacent water volumes, and $Q_{c,pipe\text{-}water}$ represents the convective thermal power exchanged between the riser pipe and the water included in the pipe riser.

The results of this modelling are shown in the following section together with the experimental validation.

2.4. Experimental validation

The novel solar thermal collector is developed at *Cyprus University of Technology* in Limassol (CY) by designing and shaping various elements suitable for standing a medium vacuum level, as illustrated in Fig. 2b. Post-construction, the system is subjected to an extensive experimental campaign in which the prototype is tested under diverse operating conditions and vacuum levels. To accurately assess the energy performance of the novel solar thermal collector, a suitable experimental setup is assembled, and the collector is tested during the period that lasted from September 13th to November 25th, 2022. This timeframe is chosen because it is the most representative period of the year in terms of solar irradiance in the region, as demonstrated in Table 2, which shows that the solar irradiance on the horizontal surface in Limassol varies from 2.40 kWh/(m^{2}day) in December to 7.64 kWh/(m^{2}day) in June.

Thus, to ensure accurate representation of energy performance under different solar irradiance and weather conditions, the months between September and November are considered suitable for testing the performance of the prototype for summer and mid-season conditions. To assess the performance of the prototype, various experimental analyses are conducted, and several parameters are measured. The analysis involved using different sensors that are connected through a selector to three different data readers, model OM-DaqPro 5300, 8 channels, with a range of utilization of 0–24 mA, a resolution of 4.76 μA, and an accuracy of ±0.50 %. The placement of these sensors is shown in Fig. 7, where temperatures, flowrates, and solar radiation measurements are obtained, according to the follow list.

i) Inlet ($T_{water,in}$), and outlet ($T_{water,out}$) water temperature flowing at the inlet and outlet of the novel solar thermal collector.
ii) Water temperature of the storage tank (T_{TNK}) that is suitably coupled to the solar thermal collector.
iii) Surface pipe temperatures at the bottom ($T_{pipe,1}$, $T_{pipe,4}$, and $T_{pipe,7}$), middle ($T_{pipe,2}$, $T_{pipe,5}$, and $T_{pipe,8}$), and top ($T_{pipe,3}$, $T_{pipe,6}$, and $T_{pipe,9}$) of the risers placed on the back of the solar thermal collector.
iv) Surface absorber temperature at the bottom ($T_{absorber,1*}$, $T_{absorber,4*}$, and $T_{absorber,7*}$), middle ($T_{absorber,2*}$, $T_{absorber,5*}$, and $T_{absorber,8*}$), and top ($T_{absorber,3*}$, $T_{absorber,6*}$, and $T_{absorber,9*}$) of the absorber placed on the back of the solar thermal collector.
v) Surface glass cover in the centre of the glass cover (T_{glass}).
vi) Outdoor air temperature for the weather boundary condition assessment.
vii) Solar radiation assessment (G_{tot}) through the adoption of a suitable Kipp and Zonen CM11 pyranometer (sensitivity: 10 μW/(W/m^2).

Table 2
Monthly distribution of solar irradiance for the weather zone of Limassol.

Month	Jan	Feb	Mar	Apr	May	Jun	Jul	Aug	Sep	Oct	Nov	Dec
[kWh/(m^{2}day)]	2.57	3.44	4.89	5.72	6.94	7.64	7.33	6.56	5.72	4.53	3.14	2.40

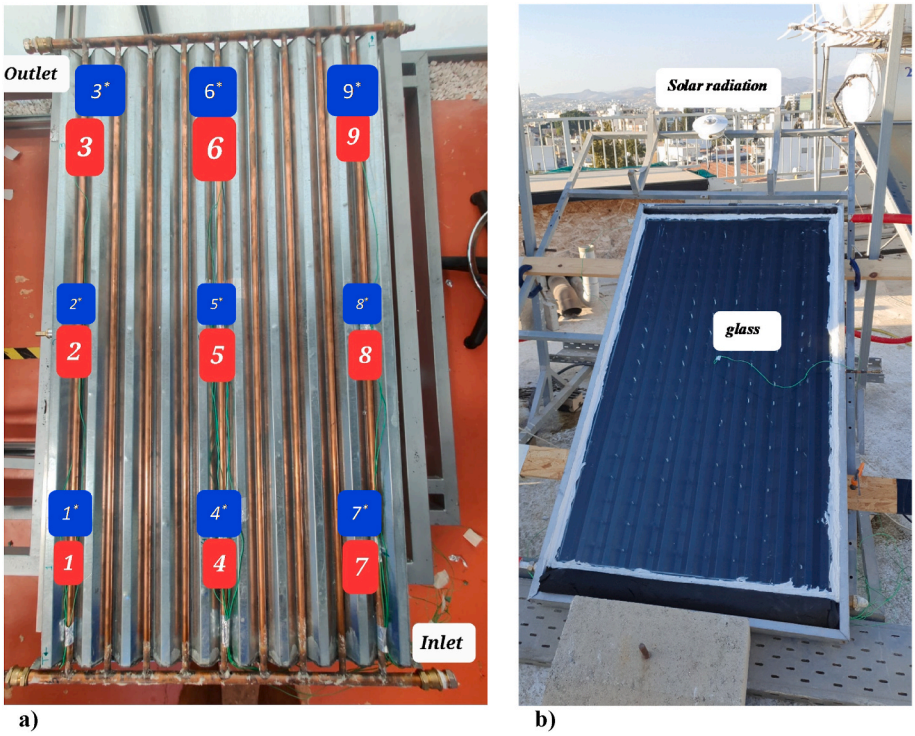

Fig. 7. Experimental setup with sensors arrangement: a) sensors placed on the back of the collector; b) sensors positioned on the front of the collector.

viii) A vacuum pump for assessing different pressure level into the gap cavity.

This section presents the results of the experimental analyses conducted and the corresponding validation of the investigated configuration system. The developed dynamic simulation model is verified against the experimental data by comparing the calculated parameters with the measured ones. These parameters include the water flow temperature at the outlet of the system ($T_{water,out}$), absorber surface temperature at the bottom, middle, and top ($T_{absorber,1}$ - $T_{absorber,9}$), surface pipe temperature ($T_{pipe,1}$ - $T_{pipe,9}$), and glass cover temperature (T_{glass}). The simulation model requires input data such as ambient air temperature (T_{amb}), incident solar radiation (G_{tot}), and wind velocity (w_{speed}) to assess these parameters. The validation procedure spanned a duration of multiple weeks, specifically from September 13th to November 25th, 2022. However, for the sake of brevity, in the following only the results pertaining to three highly significant hot days (September 15th - 18th) and three moderately significant mild days (October 19th - 21st) are reported.

Fig. 8 illustrates the time history of the ambient air temperature and the global horizontal radiation for the selected hot and mild days, where the former are depicted on the left side, and the latter are depicted on the

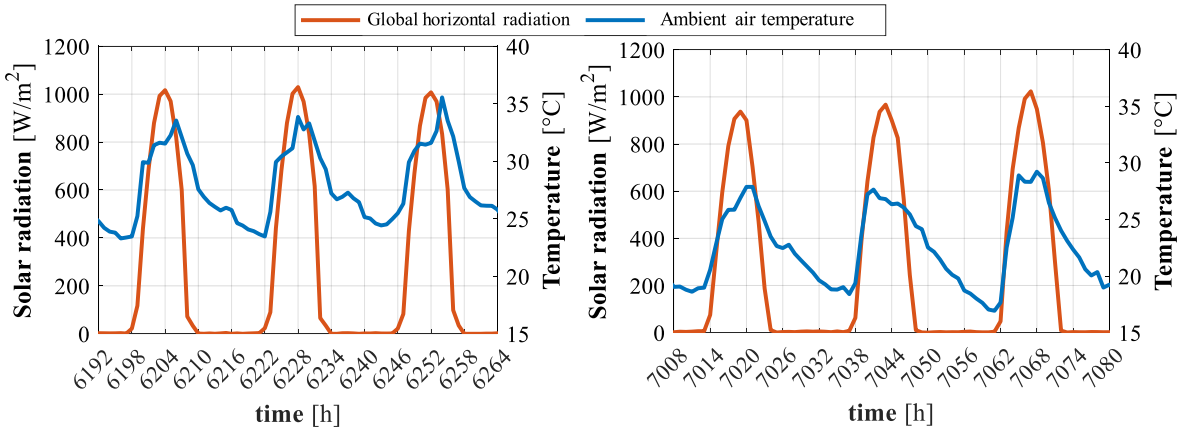

Fig. 8. Weather boundary conditions: a) September 15th - 18th; b) October 19th - 21st.

right side.

The analysis reveals that the global solar radiation exhibits a significantly high intensity, peaking at approximately 1020 W/m^2 during the Sept 16th,13:00 and at 1015 W/m^2 during the Oct 21st, 13:00. Thus, negligible variations are observed between the two sets of sample days in terms of solar radiation. However, noteworthy dissimilarities are observed in the outdoor air temperature between the three selected hot days and mild days. Specifically, the maximum outdoor air temperature during the hot days reaches 34.9 °C at the Sept 17th, 15:00, while the minimum temperature of 22.3 °C is recorded at the Sept 15th, 4:00. In contrast, the maximum outdoor air temperature during the mild days is 28.6 °C at the Oct 21st, 15:00, whereas the minimum temperature of 17.0 °C is observed at the Oct 21st, 5:00. Based on these boundary conditions, the subsequent section details the experimental validation procedure.

Figs. 9 and 10 provide a comprehensive account of the experimental validation procedure carried out on the nine temperatures obtained from the riser pipes and the nine temperatures measured on the absorber plate, respectively, against the corresponding simulated temperatures.

Fig. 9 comprises nine individual subplots, each representing the temporal evolution of the pipe riser temperatures for the selected hot days. A comparison between the measured temperatures, represented by the blue solid lines labelled as EXP, and the corresponding simulated values, denoted by the red solid lines labelled as SIM, is carried out. The comparison results demonstrate good agreement between the measured and simulated temperatures. Additionally, Fig. 9 enables a detailed assessment of the maximum temperature attained by the solar collector, whereby the riser pipes reach a peak temperature of approximately 94 °C at the September 15th, 10:00.

Similarly, Fig. 10 presents a comparative analysis of the measured and simulated temperatures for the absorber plate readings. The results indicate a high level of correspondence between the experimental measurements and the simulated values. Moreover, the absorber plate exhibits an even higher temperature, reaching approximately 102 °C at the September 15th, 10:00. Furthermore, the developed dynamic simulation model provides an effective means of evaluating the temperature distribution throughout the system.

The experimental validation results obtained for the entire experimental campaign are summarized in a suitable scatter plot reported in Fig. 11. Here, the measured temperatures are reported against the simulated ones. The scatter plot is divided into four subplots, each representing a different comparison parameter. In the top left subplot of Fig. 11, the comparison is made between the measured nine temperature of the absorber plate and the simulated ones. The plotted points on the red solid line show 0 % error, while the dotted black lines near the red line represent the points with an error of approximately ±5.0 %, and so on. The experimental results exhibit a good agreement between the measured and simulated temperatures for these parameters, with an R^2 value of approximately 0.975, a mean average error (MAE) of approximately 2.67 °C, and a mean average percentage error (MAPE) of approximately 5.82 %.

The top right subplot of Fig. 11 represents the comparison between the measured nine temperature of the riser pipes and the simulated ones. The experimental results reveal a good agreement between the measured and simulated temperatures for these parameters, with an R^2 value of approximately 0.987, a MAE of approximately 1.99 °C, and a MAPE of approximately 4.97 %. The bottom left subplot of Fig. 11 depicts the comparison between the measured temperature of the glass cover and the simulated temperature. The experimental results indicate a good agreement between the measured and simulated temperatures for these parameters, with an R^2 value of approximately 0.882, a MAE of approximately 2.25 °C, and a MAPE of approximately 7.47 %. Finally, in the bottom right subplot of Fig. 11, the comparison is made between the measured temperature of the outlet water and the simulated one. The experimental results reveal a good agreement between the measured and simulated temperatures for these parameters, with an R^2 value of approximately 0.924, a MAE of approximately 1.72 °C, and a MAPE of approximately 4.23 %.

2.5. Proof of concept

The energy performance of different versions of the novel low-cost flat plate evacuated thermal collector is experimentally tested and simulated through the dynamic simulation model. These versions of the

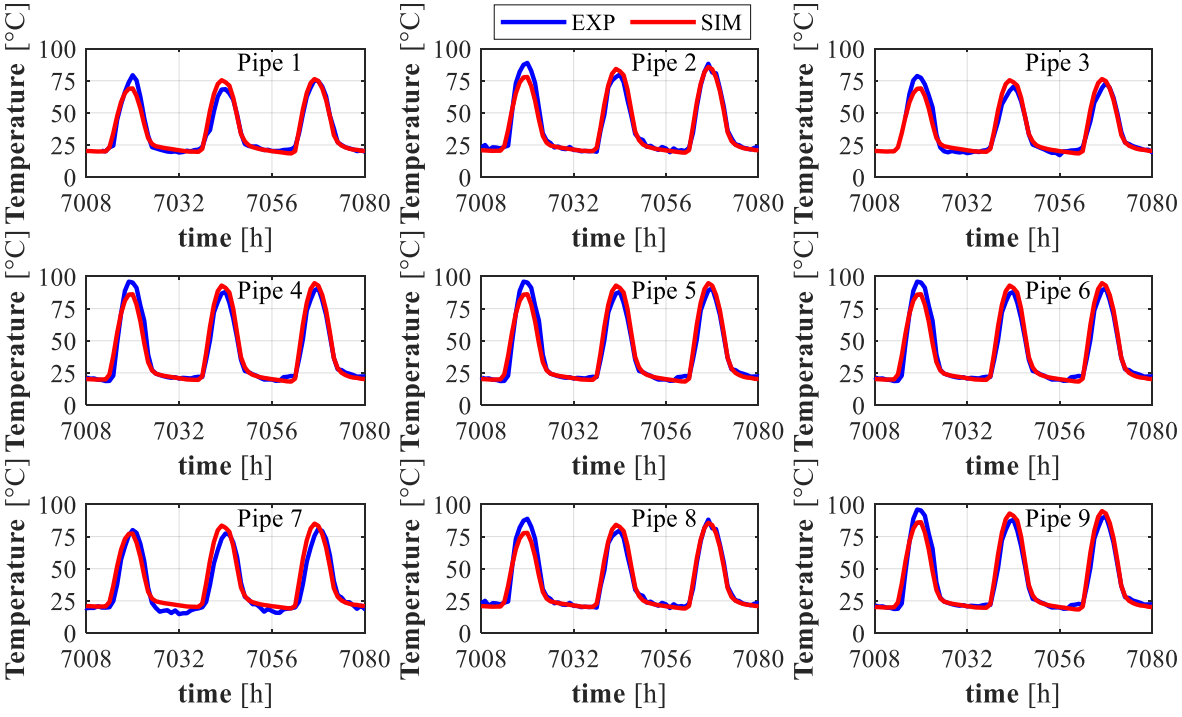

Fig. 9. Experimental validation via riser pipes temperature comparisons: for the three sample days from October 19th (7008 h) to October 21st (7080 h).

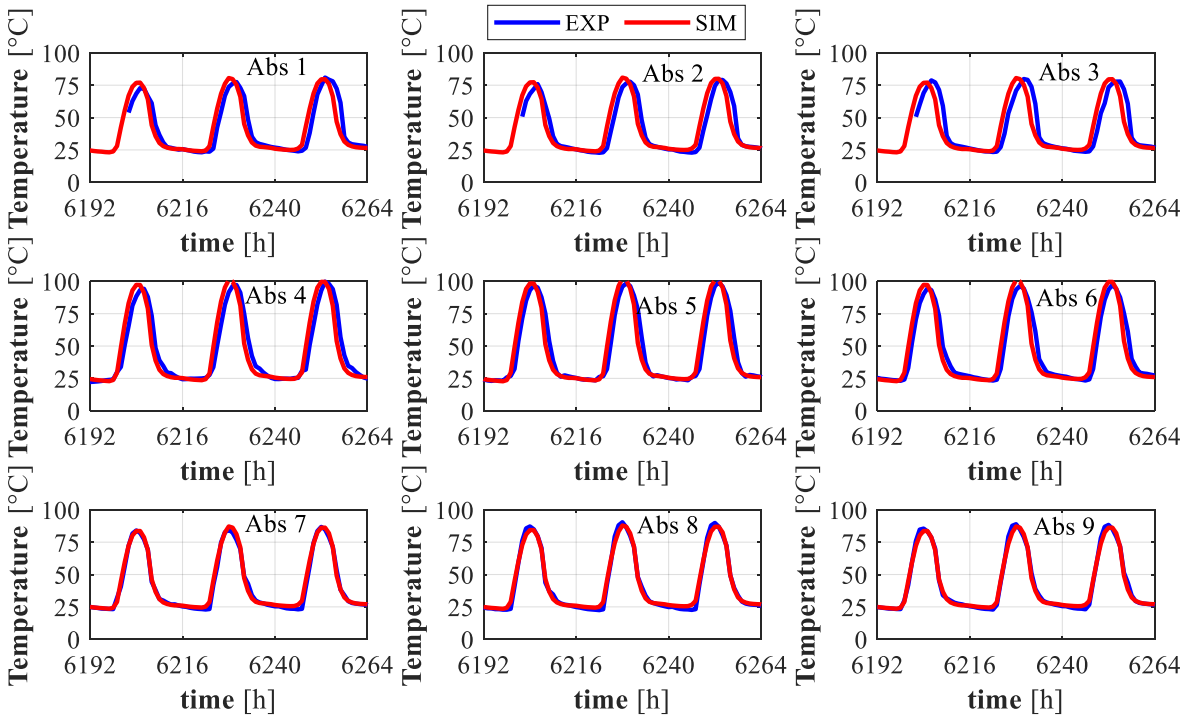

Fig. 10. Experimental validation via absorber plate temperature comparisons: for the three sample days from September 15th (6192 h) to September 18th (6264 h).

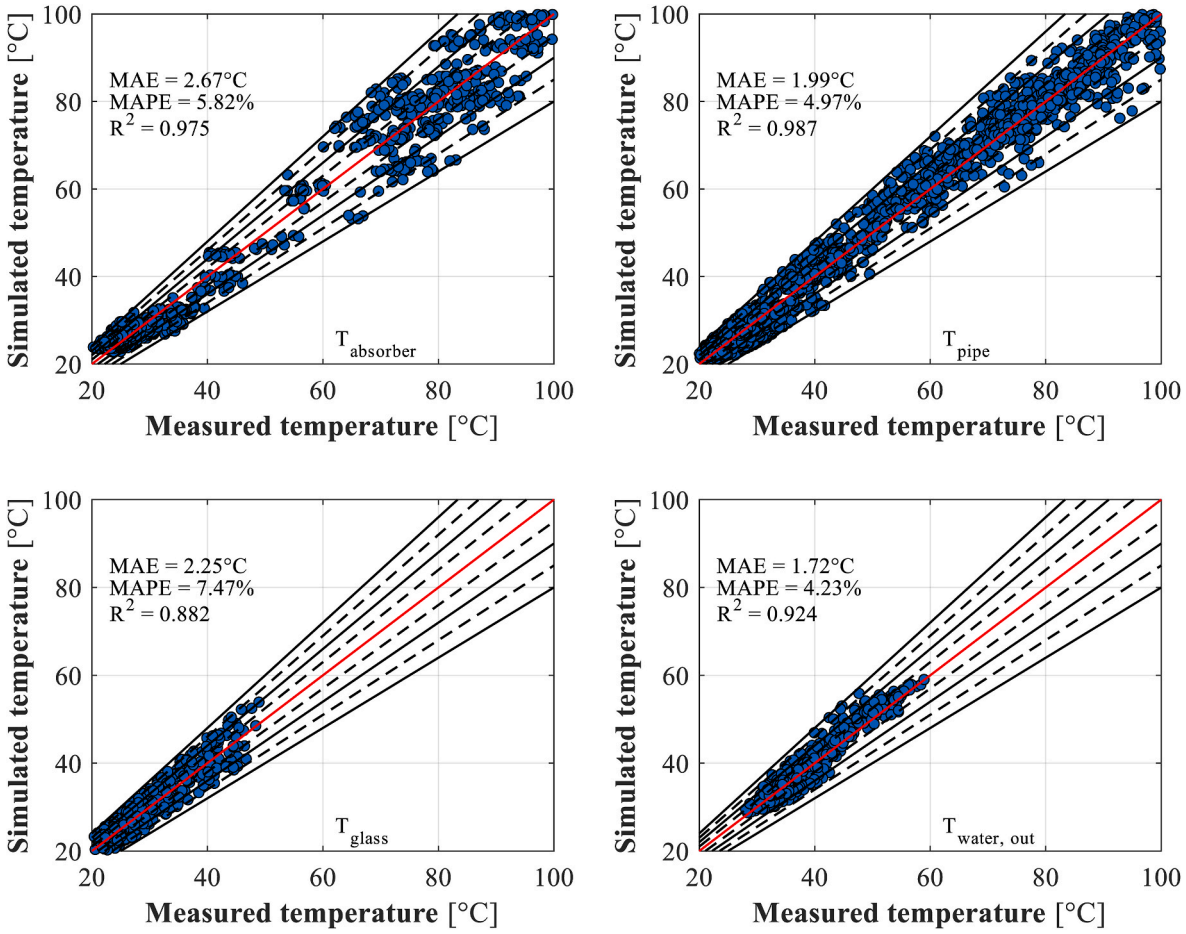

Fig. 11. Simulated vs. experimental results (for the entire period of the conducted tests).

collector are characterized by different vacuum levels occurring into the gap cavity. Specifically, five different configurations were tested: the *Ref.* Case that correspond to no vacuum level or, what is the same, a standard flat plate solar thermal collector, two low vacuum quality levels (10^{-1} and 10^{-2} mbar for *Ver.01* and *Ver.02*), and two medium vacuum quality levels (10^{-3} and 10^{-5} mbar for *Ver.02* and *Ver.03*). For each of these versions, the effects on the energy efficiency are assessed through the assessment of characteristics curves. Finally, to evaluate the environmental and economic profitability of these systems a suitable analysis is also conducted [73]. It is hypothesized to produce hot water for satisfy the domestic hot water demand of a single-family house. The novel low-cost flat plate evacuated thermal collector produces hot water for end users at about 60 °C by heating tap water at 15 °C. As a backup, a natural gas boiler with a design efficiency of 0.85 and a nominal power of 15.0 kW is also included. Furthermore, a unitary cost of natural gas (j_{NG}) of 0.80 €/Sm^3 and an emission factor related to primary energy (f_{NG}) of 0.202 kg_{CO2}/kWh_p are taken into consideration. As assumption, the electricity supplied to the water pump equipped on the solar loop is not accounted. The hourly weather conditions included in TMY2 data files form the basis of the annual simulations, which run from 0:00 on January 1st to 24:00 on December 31st [74]. The simulations are referred to the weather zone of Limassol, Cyprus, which has a global incident solar radiation of 1854 kWh/(m^2y) and 698 heating degree days.

3. Result and discussion

In the initial testing phase, the solar thermal collector underwent comprehensive evaluation without incorporating a vacuum, wherein its energy performance is assessed to establish a reference case. This approach is employed to determine a performance reference, thereby facilitating subsequent comparisons with distinct vacuum levels. The operational configuration of the system excluded any auxiliary backup, relying solely on a solar loop to supply feed water to the solar collector, seamlessly interconnected with a designated tank serving as a reservoir for hot water storage. Throughout this configuration, the system underwent a total of 346 between simulations and measurements, generating a diverse set of scatter points that are subsequently organised and shown in Fig. 12.

In the presented figure, an array of scattered points is observable, illustrating the correlation between thermal efficiency and the parameter (T_m - T_a)/G_{tot}. Here, T_m represents the average inlet and outlet water temperature, T_a is the outdoor air temperature, G_{tot} denotes the incident solar radiation on the solar thermal collector, and η_{coll} stands for the thermal efficiency, expressed as the ratio of the useful heat Q_u to the heat captured by the gross area $A_{coll} \times G_{tot}$. Notably, the configuration of the interpolation curve closely resembles that of a conventional flat-plate solar thermal collector. The intercept point, equating to 0.82, corresponds to optical losses, and thermal efficiency can be swiftly assessed through the adoption of the $\eta_{coll} = a \times \Delta T/G_{tot} + b$, where a is −17.3 W/m^2K, and b is 0.82.

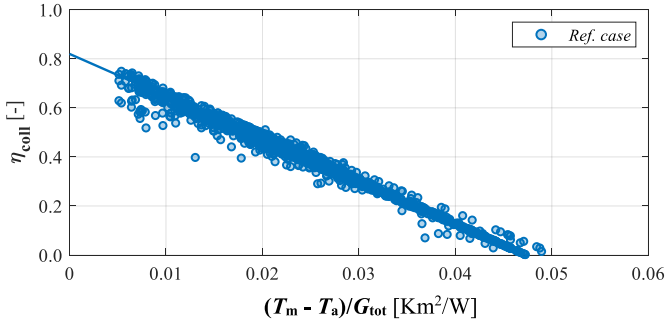

Fig. 12. Characteristic curve for *Ref.* Case – standard flat plate solar collector.

Subsequent to these observations, the experimentation extended to incorporate the integration of a suitable vacuum valve, a manometer positioned at the edge of the collector, and a vacuum pump connected to the valve to establish and regulate the vacuum level within the gap cavity between the absorber plate and the glass cover. The experimental analysis at different vacuum levels was conducted for twenty days and data was collected every minute during the sun hours, for a total of nine thousand points. Consequently, through a combined approach involving simulations and experiments, a substantial dataset comprising two thousand points was exploited, systematically plotted across four distinct graphs that characterize four different version of the evacuated flat plate solar thermal collector, as depicted in Fig. 13. In this figure, the dataset has been categorized based on varying vacuum levels, and it has been depicted across four different graphs. Each graph features a characteristic curve alongside a scattered plot specific to the corresponding vacuum quality. In each graph it is possible to distinguish the modelled and experimental assessed points with a dark and light marked edge, respectively. To elaborate, the green scattered plot and its corresponding interpolation line pertain to a low vacuum quality of approximately 10^{-1} mbar, the orange scattered plot and its relative interpolation line correspond to a low vacuum quality of approximately 10^{-2} mbar, the violet scattered plot and its associated interpolation line are indicative of a medium vacuum quality around 10^{-3} mbar, while the black scattered plot and its corresponding interpolation line represent a medium vacuum quality of about 10^{-5} mbar.

This categorization allows for a comprehensive visual examination of the relationship between vacuum quality and thermal efficiency across a diverse range of conditions. Specifically, all these graphs are characterized by the same optical losses, and this can be observed by the interception point that is equal to 0.82, as also previous assessed for the standard flat plate with no vacuum. Thus, as expected, the vacuum level does not affect the optical losses, whereas what is changing is the slope of the lines. This is more evident in Fig. 14, in which all the dataset with the interpolated characteristic curves are reported.

Upon examination of the reference case illustrated in Fig. 12, the quick assessment of energy efficiency can be performed by utilizing the characteristic curve as outlined in the following equation:

$$\eta_{coll} = a \times \frac{(T_m - T_a)}{G_{tot}} + b \tag{7b}$$

Extending this analysis to different version of the evacuated solar collector, a similar investigation can be conducted. Specifically, by analysing Fig. 14, a trend emerges: as the vacuum quality level increases, the corresponding b parameter exhibits a decrease. Notably, all interpolation lines employed for the thermal efficiency evaluation of diverse evacuated solar thermal collectors exhibit an R^2 value higher than 0.90. The parameters defining eq. (7) are reported in Table 3.

This comprehensive examination facilitates an understanding of the relationship between vacuum quality levels, the b parameter, and the ensuing thermal efficiency across different iterations of evacuated solar collectors.

Finally, to conclude the analysis of the impact of vacuum quality on the performance of solar thermal collectors, it was assumed that they would be employed to provide domestic hot water for a single-family house, as described earlier in the preceding section. The yearly energy, economic and environmental results are reported in detailed in Table 4.

Promising results in terms of primary energy, ranging from 6.4 to 12.0 %, simple pay back from 3.93 to 5.21 years, and avoided CO_2 gas emissions from 124 to 200 kg/y are achievable.

4. Conclusions

This study proposes a comprehensive approach to the design, implementation, and optimization of a novel evacuated flat-plate solar thermal collector, characterized by a vacuum level between the glass

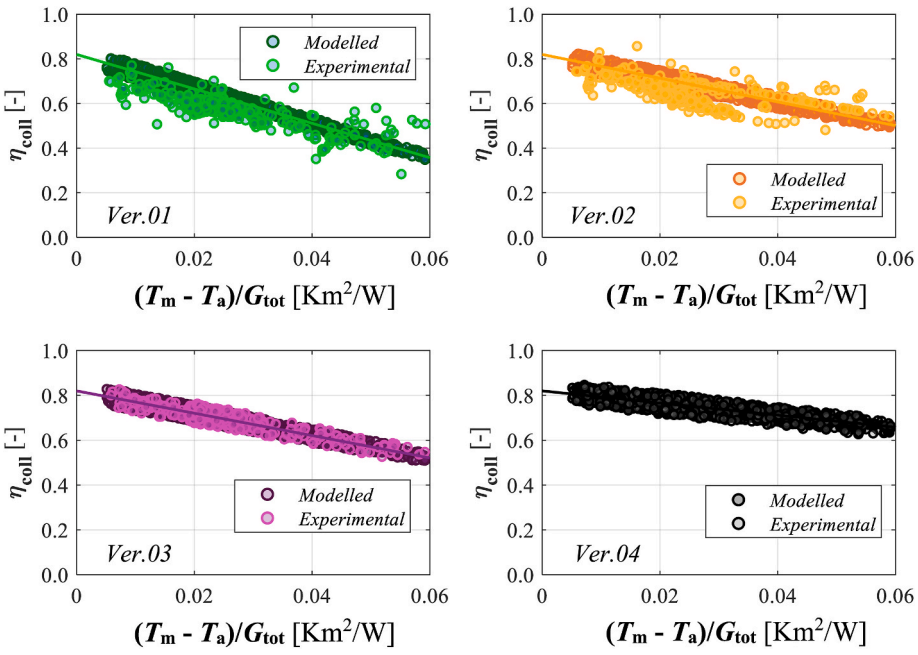

Fig. 13. Characteristic curves for evacuated flat plate solar collector with low (*Ver.01 and Ver.02*) and medium (*Ver.03 and Ver.04*) vacuum quality levels.

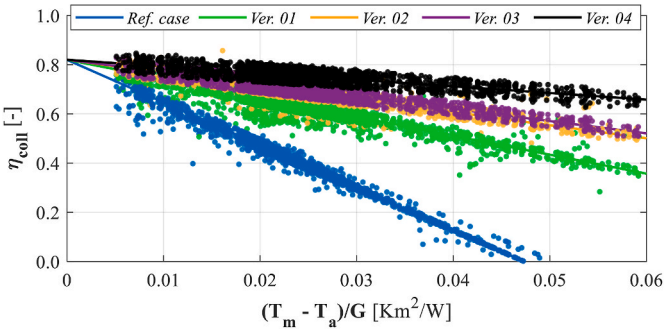

Fig. 14. Characteristic curves comparison between the standard flat plate solar collector (*Ref. case*), the evacuated flat plate solar collector with low (*Ver.01 and Ver.02*), and medium (*Ver.03 and Ver.04*) vacuum quality levels.

Table 3
Parameters characterizing characteristic curves.

		Ref. Case	Ver. 01	Ver. 02	Ver. 03	Ver. 04
Vacuum level	[–]	–	Low	Low	Medium	Medium
a	[–]	0.820	0.820	0.820	0.820	0.8200
b	[W/m^{2}K]	17.3	7.72	5.32	4.98	2.72

cover and the absorber plate. The research aimed to address the gap in existing literature by offering a methodology that covers all phases of solar thermal collector development, from conceptualization to optimization. The proposed methodology, relying on structural analysis and energy performance assessment and optimization, has proven to be reliable and effective. The innovation of this study lies in providing a thorough analysis of all production phases and showcasing a step-by-step process for designing, fabricating, testing, and optimizing a low-cost evacuated solar thermal collector.

Motivated by the need for a holistic perspective in the field, the research methodology is applied to produce a low-cost flat plate evacuated thermal collector. By incorporating a cost-effective vacuum cavity and a corrugated shape in the absorber plate, the collector demonstrated promising results. The vacuum cavity mitigated convective losses, and the corrugated shape enhanced heat exchange with pipe risers, ensuring structural integrity and preventing system implosion. In the following, the main findings of this paper are summarized.

- Development of a comprehensive and highly organised methodology that allows for the production and optimization of solar thermal collectors characterized by a high innovation level with low initial costs.
- Development of a cost-effective vacuum cavity between the absorber plate and the glass cover that significantly mitigates convective losses to the environment. Furthermore, the absorber plate has a corrugated shape that enhances the heat exchange with the pipe risers and facilitates the installation of steel pillars, thereby preventing system implosion.

Table 4
Yearly energy, economic, and environmental results.

Version	Vacuum	Q_{STC}	PE	PES	J	ΔJ	SPB	VAN	IP	ΔCO_2	
[–]	[–]	[MWh/y]			[€/y]		[y]	[€]		[kg/y]	[%]
Ref. Case	–	–	0.216	–	215	–	–	–	–	–	–
Ver.01	Low	0.54	0.152	0.064	142	73	5.21	521	1.39	124	28.3
Ver.02	Low	0.78	0.131	0.085	118	97	4.40	829	2.21	175	40.7
Ver.03	Medium	0.86	0.118	0.098	109	105	4.04	937	2.50	193	45.1
Ver.04	Medium	0.89	0.096	0.120	106	108	3.93	973	2.59	200	46.5

- Stress analysis for design the number of pillars and the thickness of glass cover able to stand different vacuum levels. A number of 144 pillars, and a glass cover about 8.0 mm are selected. For these features, a vacuum level ranging from 10^{-1} mbar (low vacuum quality) to 10^{-8} mbar (high vacuum quality) are simulated for assessing the mechanical deformation that ranges from 8.3×10^{-6} mm to 1.7×10^{1} mm.
- Dynamic simulation model able to investigate the energy, economic, and environmental performance of the considered system is developed in MatLab environment. It is experimentally validated with a good agreement between the measured and simulated temperatures. For absorber pipe temperatures, a R^2 value of approximately 0.975, a mean average error of approximately 2.67 °C, and a mean average percentage error of approximately 5.82 % are obtained.
- Four different vacuum levels were assessed, revealing promising outcomes in terms of primary energy savings, simple payback periods, and avoided CO_2 gas emissions: primary energy savings ranged from 6.4 to 12.0 %, simple payback periods varied from 3.93 to 5.21 years, and avoided CO_2 gas emissions showed a range of 124–200 kg/y.

This research contributes a reliable methodology for solar collector development and provides evidence of the positive impact of increasing vacuum levels on the thermal efficiency of solar collectors. The presented novel collector holds promise for enhanced energy efficiency, economic feasibility, and reduced environmental impact, making a valuable contribution to the advancement of sustainable energy systems.

CRediT authorship contribution statement

Giovanni Barone: Writing – review & editing, Writing – original draft, Visualization, Validation, Software, Resources, Project administration, Methodology, Investigation, Formal analysis, Data curation, Conceptualization. **Annamaria Buonomano:** Writing – review & editing, Writing – original draft, Visualization, Validation, Supervision, Software, Resources, Project administration, Methodology, Investigation, Funding acquisition, Formal analysis, Data curation, Conceptualization. **Soteris Kalogirou:** Writing – review & editing, Writing – original draft, Visualization, Validation, Supervision, Software, Resources, Project administration, Methodology, Investigation, Funding acquisition, Formal analysis, Data curation, Conceptualization. **Panayiotis Ktistis:** Writing – review & editing, Writing – original draft, Visualization, Validation, Supervision, Software, Resources, Project administration, Methodology, Investigation, Funding acquisition, Formal analysis, Data curation, Conceptualization. **Adolfo Palombo:** Writing – review & editing, Writing – original draft, Visualization, Validation, Supervision, Software, Resources, Project administration, Methodology, Investigation, Funding acquisition, Formal analysis, Data curation, Conceptualization.

Declaration of competing interest

no conflict of interest statement.

Nomenclature

Abbreviations			
EXP	experimental	θ	time (s)
MAE	mean average error	σ	mechanical stress (MPa)
MAPE	mean average percentage error		
Ref	reference case	**Subscript**	
SIM	simulated	abs	absorber
TMY	typical meteorological year	amb	ambient
Ver	version	c	convective
		coll	collector
Symbol		d	down face
A	Surface area (m^2)	edg	edge cover
C	capacitance (J/K)	gap	gap cavity
D	diameter (mm)	glass	glass
G	incident solar irradiance (W/m^2)	header	pipe heated
L	length (m)	ins	insulation
Q	thermal power (W)	k	conductive
R^2	coefficient of determination (−)	middle	middle
T	thickness (m)	pillar	pillar
T	temperature (°C)	pipe	pipe
W	width (m)	plate	absorber plate
		r	radiative
Greek Letter		sky	sky
α	absorbance (−)	tot	total
ε	mechanical deformation (mm)	u	upper face
η	thermal efficiency (−)	water	water

References

[1] IEA, World Energy Outlook 2023, 2023.
[2] Ş. Kılkış, Urban emissions and land use efficiency scenarios towards effective climate mitigation in urban systems, Renew. Sustain. Energy Rev. 167 (2022) 112733.
[3] A. Foley, B.M. Smyth, T. Pukšec, N. Markovska, N. Duić, A review of developments in technologies and research that have had a direct measurable impact on sustainability considering the Paris agreement on climate change, Renew. Sustain. Energy Rev. 68 (2017) 835–839.
[4] A.M. López-Sabirón, P. Royo, V.J. Ferreira, A. Aranda-Usón, G. Ferreira, Carbon footprint of a thermal energy storage system using phase change materials for industrial energy recovery to reduce the fossil fuel consumption, Appl. Energy 135 (2014) 616–624.
[5] O. Vojáček, L. Sobotka, J. Macháč, M. Žilka, Impact assessment of Proposal for a Directive on the limitation of emissions from medium combustion plants – national impact assessment compared to the European impact estimate, Renew. Sustain. Energy Rev. 82 (2018) 1854–1862.
[6] Z. Kyramargiou, I. Vardopoulos, Use and sustainability of the ships' waste reception facilities: evidence from the port of corinth, Greece, Rev. Bras. Gestão Desenvolv. Reg. 15 (3) (2019) 93–106.
[7] G. Barone, A. Buonomano, G. Del Papa, R. Maka, A. Palombo, How to achieve energy efficiency and sustainability of large ships: a new tool to optimize the operation of on-board diesel generators, Energy 282 (2023) 128288.

[8] A. Savvides, C. Vassiliades, Designing Urban Building Blocks Around Solar Planning Principles, 2017.
[9] S. Agostinelli, F. Nardecchia, L. Pompei, Renewable sources urban cells microgrid: a case study, International Journal of Energy Production and Management 7 (3) (2022) 207–225.
[10] A.S. Sánchez, E.P. Junior, B.M. Gontijo, P. de Jong, I.B. dos Reis Nogueira, Replacing fossil fuels with renewable energy in islands of high ecological value: The cases of Galápagos, Fernando de Noronha, and Príncipe, Renew. Sustain. Energy Rev. 183 (2023) 113527.
[11] I. Vardopoulos, Multi-criteria decision-making approach for the sustainable autonomous energy generation through renewable sources. Studying zakynthos island in Greece, Environ. Manag. Sustain. Dev. 7 (1) (2018) 33.
[12] I. Vardopoulos, I. Konstantopoulos, A.A. Zorpas, L. Limousy, S. Bennici, V. J. Inglezakis, I. Voukkali, Sustainable metropolitan areas perspectives through assessment of the existing waste management strategies, Environ. Sci. Pollut. Control Ser. 28 (19) (2021) 24305–24320.
[13] G. Barone, A. Buonomano, G.F. Giuzio, A. Palombo, Towards zero energy infrastructure buildings: optimal design of envelope and cooling system, Energy 279 (2023) 128039.
[14] Z. Ekim, P. Mattsson, R. Bernardo, Assessments of users' interactions with energy-efficient solutions: a systematic review, Build. Environ. 242 (2023) 110522.
[15] A. Buonomano, C. Forzano, L. Mongibello, A. Palombo, G. Russo, Optimising low-temperature district heating networks: A simulation-based approach with experimental verification, Energy 304 (2024) 131954.
[16] I. Vardopoulos, I. Vannas, G. Xydis, C. Vassiliades, Homeowners' perceptions of renewable energy and market value of sustainable buildings, Energies 16 (10) (2023) 4178.
[17] J. Yan, L. Lu, T. Ma, Y. Zhou, C.Y. Zhao, Thermal management of the waste energy of a stand-alone hybrid PV-wind-battery power system in Hong Kong, Energy Convers. Manag. 203 (2020) 112261.
[18] E. Rusu, Assessment of the wind power dynamics in the North Sea under climate change conditions, Renew. Energy 195 (2022) 466–475.
[19] O. Todorov, K. Alanne, M. Virtanen, R. Kosonen, A novel data management methodology and case study for monitoring and performance analysis of large-scale ground source heat pump (GSHP) and borehole thermal energy storage (BTES) system, Energies 14 (6) (2021) 1523.
[20] F. Nardecchia, L. Pompei, E. Egidi, R. Faneschi, G. Piras, Exergoeconomic and environmental evaluation of a ground source heat pump system for reducing the fossil fuel dependence: a case study in rome, Energies 16 (17) (2023) 6167.
[21] H. Ek Fälth, N. Mattsson, L. Reichenberg, F. Hedenus, Trade-offs between aggregated and turbine-level representations of hydropower in optimization models, Renew. Sustain. Energy Rev. 183 (2023) 113406.
[22] A. Trivedi, V. Trivedi, K.K. Pandey, O. Chichi, An interpretive model to assess the barriers to ocean energy toward blue economic development in India, Renew. Energy 211 (2023) 822–830.
[23] R. Wang, Z. He, H. Chen, S. Guo, S. Zhang, K. Wang, M. Wang, S.-H. Ho, Enhancing biomass conversion to bioenergy with machine learning: gains and problems, Sci. Total Environ. 927 (2024) 172310.
[24] S. Kuşkaya, F. Bilgili, E. Muğaloğlu, K. Khan, M.E. Hoque, N. Toguç, The role of solar energy usage in environmental sustainability: fresh evidence through time-frequency analyses, Renew. Energy 206 (2023) 858–871.
[25] P.A. Østergaard, N. Duic, Y. Noorollahi, S. Kalogirou, Advances in renewable energy for sustainable development, Renew. Energy 219 (2023) 119377.
[26] A. Modi, F. Bühler, J.G. Andreasen, F. Haglind, A review of solar energy based heat and power generation systems, Renew. Sustain. Energy Rev. 67 (2017) 1047–1064.
[27] L. Evangelisti, R. De Lieto Vollaro, F. Asdrubali, Latest advances on solar thermal collectors: a comprehensive review, Renew. Sustain. Energy Rev. 114 (2019) 109318.
[28] F. Sallaberry, R. Pujol-Nadal, A.G. de Jalón, V. Martínez-Moll, Toward a standard testing methodology for solar thermal collectors with variable-geometry: the direct radiation incidence angle modifier issue, Sol. Energy 121 (2015) 31–40.
[29] S. Anand, S. Kumar, Optimization of gaseous working fluid and internally finned absorber tube for enhancing the thermal performance of parabolic trough solar collector, Appl. Therm. Eng. 239 (2024) 122078.
[30] E.D. Rounis, A. Athienitis, T. Stathopoulos, Review of air-based PV/T and BIPV/T systems - performance and modelling, Renew. Energy 163 (2021) 1729–1753.
[31] P. Martínez-Merino, P. Estellé, R. Alcántara, I. Carrillo-Berdugo, J. Navas, Thermal performance of nanofluids based on tungsten disulphide nanosheets as heat transfer fluids in parabolic trough solar collectors, Sol. Energy Mater. Sol. Cell. 247 (2022) 111937.
[32] S.A. Kalogirou, Chapter three - solar energy collectors, in: S.A. Kalogirou (Ed.), Solar Energy Engineering, Academic Press, Boston, 2009, pp. 121–217.
[33] E. Vengadesan, R. Senthil, A review on recent developments in thermal performance enhancement methods of flat plate solar air collector, Renew. Sustain. Energy Rev. 134 (2020) 110315.
[34] M.S. Hossain, R. Saidur, H. Fayaz, N.A. Rahim, M.R. Islam, J.U. Ahamed, M. M. Rahman, Review on solar water heater collector and thermal energy performance of circulating pipe, Renew. Sustain. Energy Rev. 15 (8) (2011) 3801–3812.
[35] X. Yu, Z. Guo, Z. Gao, B. Yang, X. Ma, S. Dong, Thermodynamic investigation of a direct-expansion solar assisted heat pump with evacuated tube collector-evaporator, Renew. Energy 206 (2023) 418–427.
[36] Z. Ioannidis, A. Buonomano, A.K. Athienitis, T. Stathopoulos, Modeling of double skin façades integrating photovoltaic panels and automated roller shades: analysis of the thermal and electrical performance, Energy Build. 154 (2017) 618–632.
[37] G. Barone, C. Vassiliades, C. Elia, A. Savvides, S. Kalogirou, Design optimization of a solar system integrated double-skin façade for a clustered housing unit, Renew. Energy 215 (2023) 119023.
[38] Latest Updated Report, reportSolar Thermal Collector Market - Research Report Analysis and Viewpoint Insights, 2023.
[39] M. Raisul Islam, K. Sumathy, S. Ullah Khan, Solar water heating systems and their market trends, Renew. Sustain. Energy Rev. 17 (2013) 1–25.
[40] M. Nájera-Trejo, I.R. Martin-Domínguez, J.A. Escobedo-Bretado, Economic feasibility of flat plate vs evacuated tube solar collectors in a combisystem, Energy Proc. 91 (2016) 477–485.
[41] L.A. Omeiza, M. Abid, A. Dhanasekaran, Y. Subramanian, V. Raj, K. Kozak, U. Mamudu, A.K. Azad, Application of solar thermal collectors for energy consumption in public buildings – an updated technical review, J. Eng. Res. (2023). https://doi.org/10.1016/j.jer.2023.09.011.
[42] V. Shemelin, T. Matuška, Quantitative review on recent developments of flat-plate solar collector design. Part 1: front-side heat loss reduction, Energy Rep. 9 (2023) 64–69.
[43] S. Aggarwal, R. Kumar, D. Lee, S. Kumar, T. Singh, A comprehensive review of techniques for increasing the efficiency of evacuated tube solar collectors, Heliyon 9 (4) (2023) e15185.
[44] T. Beikircher, M. Möckl, P. Osgyan, G. Streib, Advanced solar flat plate collectors with full area absorber, front side film and rear side vacuum super insulation, Sol. Energy Mater. Sol. Cell. 141 (2015) 398–406.
[45] G. Barone, A. Buonomano, V. Palmieri, A. Palombo, A prototypal high-vacuum integrated collector storage solar water heater: experimentation, design, and optimization through a new in-house 3D dynamic simulation model, Energy 238 (2022) 122065.
[46] B.W. Riemer, D.L. Conner, D.J. Strickler, D.E. Williamson, Iter vacuum vessel dynamic stress analysis of a disruption, in: K. Herschbach, W. Maurer, J.E. Vetter (Eds.), Fusion Technology 1994, Elsevier, Oxford, 1995, pp. 791–794.
[47] M. Ahmadlouydarab, T.D. Anari, A. Akbarzadeh, Experimental study on cylindrical and flat plate solar collectors' thermal efficiency comparison, Renew. Energy 190 (2022) 848–864.
[48] A. Bertocco, M. Bruno, E. Armentani, L. Esposito, M. Perrella, Stress relaxation behavior of additively manufactured polylactic acid (PLA), Materials 15 (10) (2022) 3509.
[49] R.P. Garcia, S.d.R. Oliveira, V.L. Scalon, Thermal efficiency experimental evaluation of solar flat plate collectors when introducing convective barriers, Sol. Energy 182 (2019) 278–285.
[50] Y. Xia, X. Lin, Y. Shu, Z. Cheng, Enhanced thermal performance of a flat-plate solar collector inserted with porous media: a numerical simulation study, Therm. Sci. Eng. Prog. 44 (2023) 102063.
[51] A. Thakur, S. Kumar, P. Kumar, S. Kumar, A.K. Bhardwaj, A review on the simulation/CFD based studies on the thermal augmentation of flat plate solar collectors, Mater. Today: Proc. 46 (2021) 8578–8585.
[52] S. Aghakhani, M. Afrand, A. Karimipour, R. Kalbasi, M. Mehdi Razzaghi, Numerical and experimental study of thermal efficiency of a spiral flat plate solar collector by changing the spiral diameter, flow rate, and pipe diameter, Sustain. Energy Technol. Assessments 53 (2022) 102353.
[53] S. Singh, A. Kumar, A. Yadav, Experimental investigation of thermal performance evaluation of solar flat plate collector, Mater. Today: Proc. 24 (2020) 1533–1540.
[54] R. Hendawi, A. Ciftja, G. Stokkan, L. Arnberg, M. Di Sabatino, The effect of preliminary heat treatment on the durability of reaction bonded silicon nitride crucibles for solar cells applications, J. Cryst. Growth 542 (2020) 125670.
[55] S. Chowdhury, Fabrication of polymeric vacuum-sealed cavities on a silicon wafer, Microelectron. Reliab. 138 (2022) 114689.
[56] F. Arya, T. Hyde, P. Henshall, P. Eames, R. Moss, S. Shire, J. Uhomoibhi, Fabrication analysis of flat vacuum enclosures for solar collectors sealed with Cerasolzer 217, Sol. Energy 220 (2021) 635–649.
[57] E.M. Abo-Zahhad, S. Memon, A. Radwan, M.R. Elmarghany, A. Khater, C. Ghenai, O. Abdelrehim, A new fusion-edge sealed vacuum for concentrated photovoltaic/thermal solar collector in comparison to a conventional system, Case Stud. Therm. Eng. 34 (2022) 102003.
[58] L. Zhang, S. Zhang, P. Joshi, M. Bhandari, A. Hu, S. Shin, Laser strengthening of additive manufactured edge seal for vacuum insulated glazing with micro-size glass frit, J. Build. Eng. 53 (2022) 104539.
[59] H. Kind, E. Gehlen, M. Aden, A. Olowinsky, A. Gillner, Laser glass frit sealing for encapsulation of vacuum insulation glasses, Phys. Procedia 56 (2014) 673–680.
[60] A. Radwan, O. Abdelrehim, M.S. Salem, E.M. Abo-Zahhad, M.R. Elmarghany, M. A. Shouman, A. Khater, A modified support pillar design for a flat vacuum-based solar thermal collectors, Sustain. Energy Technol. Assessments 58 (2023) 103372.
[61] I. Visa, M. Moldovan, A. Duta, Novel triangle flat plate solar thermal collector for facades integration, Renew. Energy 143 (2019) 252–262.
[62] A. Seddaoui, M.Z. Dar Ramdane, R. Noureddine, Performance investigation of a new designed vacuum flat plate solar water collector: a comparative theoretical study, Sol. Energy 231 (2022) 936–948.
[63] D. Gao, J. Li, X. Ren, T. Hu, G. Pei, A novel direct steam generation system based on the high-vacuum insulated flat plate solar collector, Renew. Energy 197 (2022) 966–977.
[64] L. Martínez-Manuel, N.G. González-Canché, L.B. López-Sosa, J.G. Carrillo, W. Wang, C.A. Pineda-Arellano, F. Cervantes, J.J.A. Gil, M.I. Peña-Cruz, A comprehensive analysis of the optical and thermal performance of solar absorber coatings under concentrated flux conditions, Sol. Energy 239 (2022) 319–336.
[65] Y. Xue, Z. Huang, X. Yang, J. Zhao, H. Zhang, G. Zhang, A. Guo, L. Yan, F. Hou, J. Liu, High temperature-resistant flexible inorganic coating for aluminium silicate

fiber cloth with low solar absorption ratio and high emissivity, Ceram. Int. 49 (9) (2023) 13799–13806. Part A.
[66] S. Maqsood, Z. Ali, K. Ali, M. Ishaq, M. Sajid, A. Farhan, A. Rahdar, S. Pandey, Assessment of different optimized anti-reflection coatings for ZnO/Si heterojunction solar cells, Ceram. Int. 49 (23) (2023) 37118–37126. Part A.
[67] M.S. Mozumder, A.-H.I. Mourad, H. Pervez, R. Surkatti, Recent developments in multifunctional coatings for solar panel applications: a review, Sol. Energy Mater. Sol. Cell. 189 (2019) 75–102.
[68] M. Singh M, M. Kumar, P. Sivaiah, V. G, A. Kumar, D. Kumar, S. Pandey, A. K. Singh, A.F. Deifalla, S.M.M. Hasnain, Simulation of metal ceramic single layer coatings for solar energy applications, Materials Science for Energy Technologies 7 (2024) 85–90.
[69] E. Svinterikos, I. Zuburtikudis, H. Abu Khalifeh, S. Farvin Akbar Ali, Multifunctional polymer-based coatings for outdoor glass surfaces: a state of the art, Advanced Industrial and Engineering Polymer Research 6 (3) (2023) 310–332.
[70] Creo Parametric 3D Modeling Software. https://www.ptc.com/en/products/creo/parametric.
[71] ANSYS Workbench Platform software. https://www.ansys.com/products/ansys-workbench.
[72] A. Buonomano, U. Montanaro, A. Palombo, S. Santini, Dynamic building energy performance analysis: a new adaptive control strategy for stringent thermohygrometric indoor air requirements, Appl. Energy 163 (2016) 361–386.
[73] P. Mazzei, A. Palombo, Economic evaluation of hybrid evaporative technology implementation in Italy, Build. Environ. 34 (5) (1999) 571–582.
[74] L. Bellia, P. Mazzei, A. Palombo, Weather data for building energy cost-benefit analysis, Int. J. Energy Res. 22 (14) (1998) 1205–1215.